MRI of Shoulder Disorders

Colm J. McMahon[1]

The human shoulder provides an important balance of mobility and stability, permitting loading and power transfer under a great variety of positions and situations critical to normal daily activity, sport, and occupational tasks. Consequently, shoulder disorders are an important cause of disability, lost productivity [1], sick-leave costs, and healthcare costs [2].

Shoulder symptoms are highly prevalent, with about half of adults experiencing at least one episode of shoulder pain on a yearly basis [3]. In addition to sporting injury and acute trauma, shoulder injury may occur due to work-related stresses, such as heavy lifting, working above shoulder height, repetitive movements, vibration, and suboptimal postures [4, 5]. Rotator cuff injury should also be considered in patients following acute trauma, with a substantial incidence in patients presenting to emergency departments with shoulder pain and negative radiographs following trauma [6]. Rotator cuff disease increases in prevalence with age, with about 10% prevalence in patients under 20 years of age, and 60% in patients over 80 years of age [7].

In recent years, increasing numbers of patients are presenting with rotator cuff injury and are undergoing surgical repair of rotator cuff tears with reasons cited including increased diagnostic capability of imaging techniques, increased numbers of orthopedic surgeons trained in arthroscopy, and a growing number of older and physically active patients [8, 9]. Despite the increased healthcare cost incurred by increased surgical intervention, economic models show an overall societal cost savings associated with surgical repair of full thickness rotator cuff tears [10]. Physical therapy is an important adjunctive and sometimes alternative therapy for rotator cuff tears [11].

With the high prevalence of shoulder disorders and cost-effective management requiring accurate diagnosis, awareness of shoulder MRI protocols, anatomy, and diagnostic approaches are essential for the practicing radiologist.

Imaging Protocol

In general, MRI protocols of the shoulder at Beth Israel Deaconess Medical Center fall into two categories: MRI arthrogram, performed when labral pathology is a primary clinical concern, and unenhanced MRI shoulder (without arthrogram) in all other cases. Where there is a specific question of bone or soft-tissue mass, imaging protocols are different and include the use of IV gadolinium, with imaging planes and FOV optimized to the suspected mass. Soft tissue and bone mass imaging are beyond the scope of this review.

MRI Arthrogram

Before MRI, intraarticular injection of gadobutrol (Gadovist, Bayer Schering Pharma) diluted with saline (1:200) is performed in the fluoroscopy suite. Then, within a short time period (generally less than 20 minutes) the patient undergoes MRI. The protocol includes fat-suppressed T1-weighted imaging in three planes to maximize the contrast-to-noise ratio provided by intraarticular contrast. Coronal T1-weighted and fat-suppressed T2-weighted imaging completes the protocol. Fat-suppressed T2-weighted images provide fluid sensitivity, permitting assessment of marrow edema and periarticular fluid including bursal fluid distention and acromioclavicular effusion. T2-weighted images also allow detection of tendinosis and bursal and intrasubstance rotator cuff tears, which are relatively occult on T1-weighted images. T1-weighted images provide an assessment of normal bone marrow signal and muscle quality. Of note, coronal images are angled obliquely, paralleling the plane of the supraspinatus, prescribed with reference to the axial images. Full MRI arthrogram parameters are shown in Table 1.

MRI Shoulder (Without Arthrogram)

This protocol comprises an initial axial proton density (PD)-weighted series with fat suppression, with relatively long TE compared with conventional PD, of about 35–40 ms. This intermediate weighting provides relatively good fluid sensitivity and increases the contrast-to-noise ratio for cartilage evaluation. Prescribed with respect to the axial images, oblique coronal fat-suppressed T2-weighted images are then acquired, parallel to the long axis of the supraspinatus as seen on axial images. At our institution, coronal PD images are no longer acquired due to limited utility in rotator cuff evaluation due to the magic angle effect [12, 13]. Finally, sagittal T1 and fat-suppressed T2-weighted images are prescribed, orthogonal to the coronal oblique images. This provides an evaluation for normal bone marrow and also permits assessment of rotator cuff muscle quality. Full MRI parameters are shown in Table 2.

[1]Department of Radiology, Beth Israel Deaconess Medical Center, 330 Brookline Ave, Boston, MA 02215. Address correspondence to C. McMahon (cmcmahon@bidmc.harvard.edu).

Shoulder Anatomy

In this section, anatomy will be described in the order in which it is routinely reviewed by the author, to facilitate systematic approach to interpretation.

Long Head of Biceps Tendon

This is seen on axial images as a round or ovoid low–signal-intensity structure within the intertubercular groove, between the greater and lesser tuberosities. The tendon is deep to the transverse ligament, a superficial extension of the distal subscapularis fibers. The tendon often has a small amount of fluid around it within the biceps tendon sheath. On occasion, a low–signal-intensity structure is seen extending from the biceps sheath to the tendon itself – this is an embryologic remnant related to invagination of the developing tendon sheath by the tendon itself, referred to as the biceps mesotendon. Superior to the intertubercular groove, the tendon curves through the rotator interval between the supraspinatus and subscapularis tendons into the shoulder joint (intraarticular portion) to merge with the superior glenoid labrum (biceps-labral anchor) and attach at the supraglenoid tubercle. The tendon within the rotator interval and its intraarticular portions are best seen on sagittal and coronal images.

Subscapularis

This is well seen using a combination of axial and sagittal images. The muscle originates from the anterior surface of the scapular body and passes laterally to form a broad tendon, which attaches into the lesser tuberosity. The myotendinous junction of the subscapularis tendon is more laterally positioned at the inferior fibers compared with the mid and superior fibers. The inferior fibers therefore have a more muscular insertion than the tendinous insertion of the superior fibers. The tendon should be evaluated on axial images where it is seen in the long axis as well as sagittal images where it is assessed in the short axis. As with other tendons, in normal circumstances, the tendon usually has a quite uniformly low signal on all sequences.

Supraspinatus

This originates from the supraspinatus fossa at the superior aspect of the scapula, above the scapular spine. The tendon attaches to the anterior portion of the greater tuberosity over an anterior-to-posterior distance of about 2 cm. The tendon is well seen on coronal images in its long axis, and sagittal fluid-sensitive images are invaluable for assessment of tear morphology and size. One challenge in evaluation of the supraspinatus tendon is the varied position and orientation of the tendon depending on the patient's internal and external shoulder position. Ideally, the patient should be scanned in a neutral position, with the palm facing anteriorly. Excessive rotation can lead to the tendon being outside the plane of the oblique coronal images. It is essential to be cognizant of the effect of patient position on the supraspinatus tendon position relative to other structures. One helpful safeguard is to always commence assessment of the tendon from the anterior-most aspect of the greater tuberosity, immediately posterior to the biceps tendon. This helps avoid the pitfall of missing isolated anterior leading-edge supraspinatus tears.

TABLE 1: MRI Arthrogram Parameters

Sequence	TR/TE	FOV (cm^2)	ST (mm)	Matrix
Axial T1 FS	600/9	12–14	3.5	256 × 256
Coronal T1 FS	600/9	12–14	3.0	256 × 256
Sagittal T1 FS	600/9	12–14	3.5	256 × 256
Coronal T2 FS	5000/65	12–14	3.0	256 × 256
Coronal T1	450/9	12–14	3.5	256 × 256

Note—FS = fat-suppression, ST = slice thickness.

TABLE 2: MRI Shoulder (Without Arthrogram) Parameters

Sequence	TR/TE	FOV (cm^2)	ST (mm)	Matrix
Axial PD FS	3000/35	12–14	3.5	256 × 256
Coronal T2 FS	4000/65	12–14	3.5	256 × 256
Sagittal T2 FS	4000.65	12–14	4.0	256 × 256
Sagittal T1	450/9	12–14	4.0	256 × 256

Note—PD = proton density, FS = fat-suppression, ST = slice thickness.

Infraspinatus

The infraspinatus originates along the posterior aspect of the scapula, inferior to the scapular spine. The tendon inserts on the posterior-superior aspect of the greater tuberosity. The anterior infraspinatus tendon fibers merge with posterior supraspinatus fibers at their insertion. This portion of overlap is referred to as the conjoint tendon. The infraspinatus fibers can be recognized by the direction of fiber orientation, extending from the more-posterior infraspinatus myotendinous junction. The appearance can vary somewhat depending on degree of shoulder rotation. As on evaluation of the supraspinatus, sagittal images are important to characterize and localize infraspinatus tendon tears and to distinguish anatomically from the adjacent supraspinatus fibers.

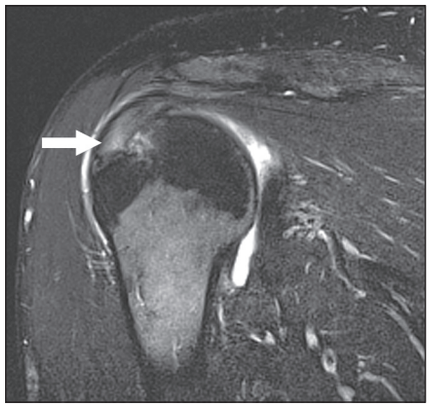

Fig. 1—Coronal fat-suppressed T2-weighted image shows diffusely increased signal intensity within infraspinatus tendon (*arrow*) due to tendinosis.

Teres Minor

The teres minor originates from the inferior aspect of the posterior scapula, inferior to the infraspinatus origin, with a tendon extending laterally to insert on the inferior aspect of the posterior greater tuberosity. The tendon is relatively small compared with the remaining rotator cuff tendons and is seldom injured in isolation.

Rotator Cuff Muscles

The rotator cuff muscles are usually intermediate in signal on T1- and T2-weighted images, with the myotendinous junctions forming laterally, and extending into their tendons. Muscle atrophy and denervation are discussed later in this chapter.

Subacromial Bursa

This is a thin synovial-lined potential space located superficial to the rotator cuff tendons. This contains minimal to no fluid under normal circumstances, and there is a thin layer of fibroadipose tissue superficial and deep to it.

Glenoid Labrum

The labrum is a ringlike fibrocartilaginous structure that encircles the rim of the glenoid, deepening and adding stability to the glenoid. The labrum is triangular when viewed in cross section and is best assessed on axial and coronal images. The labrum is typically tightly in apposition with the glenoid cartilage. There are some important normal variations of labral anatomy to be aware of. At the anterior aspect of the superior labrum, there may be an anatomic recess or foramen between the labrum and the glenoid, termed the sublabral recess or sublabral foramen, respectively. These variants are usually located anterior to the biceps-labral anchor and may extend into the anterior-superior labrum but not below the mid anterior labrum. Normal sublabral recesses are smooth and parallel the glenoid cortex, extending from inferolateral to superomedial in direction. A further variant is a Buford complex, whereby the anterior labrum is developmentally very diminutive and anterior stability is supported by an enlarged middle glenohumeral ligament. This should not be mistaken for a labral tear.

Glenohumeral Joint

Under normal circumstances, a smooth layer of cartilage is present at the glenoid and humeral head. A small volume of fluid is contained within the joint physiologically. The glenohumeral synovium is usually thin, smooth, and imperceptible on unenhanced MRI. The shoulder is supported by glenohumeral ligaments superiorly, anteriorly (the middle glenohumeral ligament), and inferiorly.

Acromioclavicular Joint

This synovial joint is a simple diarthrodial joint with thin synovium and minimal fluid under normal circumstances. A capsule connects the distal clavicle to the acromion. Stability is assisted by coracoclavicular ligaments extending from the coracoid process of the scapula to the undersurface of the clavicle.

Tendon Disorders

Tendinosis

Healthy human tendons are composed of tightly packed parallel bundles of collagen fibers with minimal cellularity in the form of tenocytes. This explains the normal hypointensity of tendons on T2-weighted imaging. Tendinosis is a condition in which degeneration occurs as a consequence of

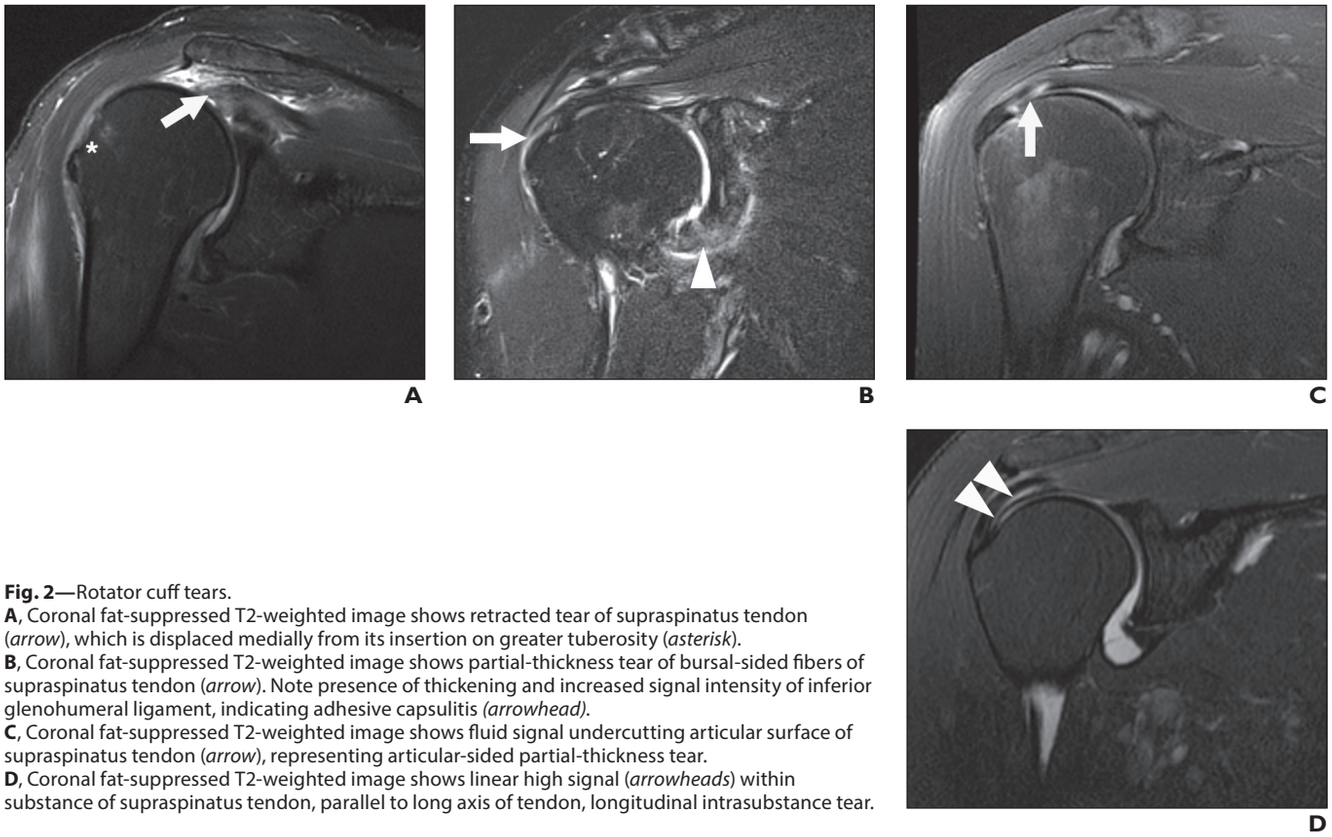

Fig. 2—Rotator cuff tears.
A, Coronal fat-suppressed T2-weighted image shows retracted tear of supraspinatus tendon (*arrow*), which is displaced medially from its insertion on greater tuberosity (*asterisk*).
B, Coronal fat-suppressed T2-weighted image shows partial-thickness tear of bursal-sided fibers of supraspinatus tendon (*arrow*). Note presence of thickening and increased signal intensity of inferior glenohumeral ligament, indicating adhesive capsulitis *(arrowhead)*.
C, Coronal fat-suppressed T2-weighted image shows fluid signal undercutting articular surface of supraspinatus tendon (*arrow*), representing articular-sided partial-thickness tear.
D, Coronal fat-suppressed T2-weighted image shows linear high signal (*arrowheads*) within substance of supraspinatus tendon, parallel to long axis of tendon, longitudinal intrasubstance tear.

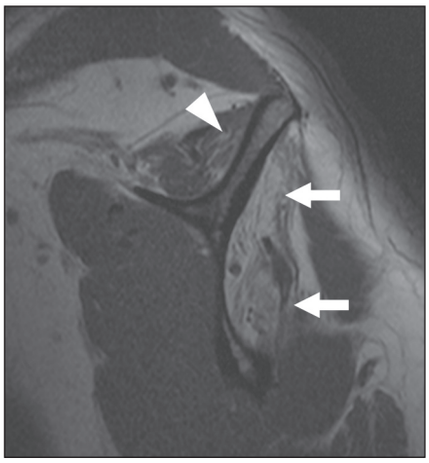

Fig. 3—Sagittal T1-weighted image shows rotator cuff muscle atrophy of varying severity. Supraspinatus muscle (*arrowhead*) shows mild loss of volume and increased fat deposition (Goutallier grade 1). Infraspinatus muscle (*arrows*) shows severe atrophy with marked fatty replacement (Goutallier grade 4).

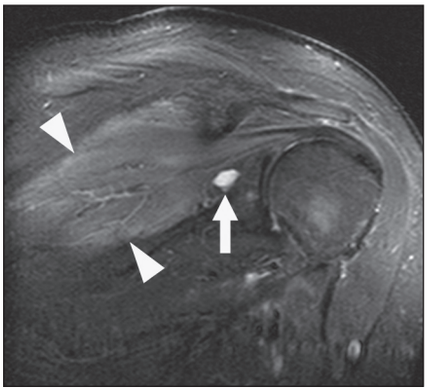

Fig. 4—Coronal STIR image shows paralabral cyst (*arrow*) within spinoglenoid notch. Mass effect on suprascapular nerve in this location results in selective denervation of infraspinatus muscle (*arrowheads*), showing increased signal early in course of denervation.

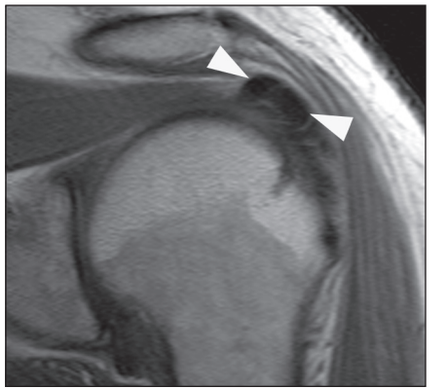

Fig. 5—Coronal proton density–weighted image shows large ovoid area of low signal (*arrowheads*) within infraspinatus tendon, corresponding with calcium deposition in setting of calcific tendinitis.

overuse. In this scenario, there is microscopic collagen bundle discontinuity and disorganization. There is a histologic increase in mucoid ground substance within the tendon, and tenocytes expand and become more chondroid in appearance (termed "fibrocartilaginous metaplasia"). Increased fibroblastic cells are seen in addition to capillary proliferation [14]. These changes lead to an increase in water content and therefore an increase in signal (Fig. 1) on T2-weighted images [15, 16]. Of note, inflammatory cells are absent in tendinosis, so the term tendinitis is not accurate for this condition. An important and well-known pitfall in interpretation is artifactual signal increase on short TE sequences (T1 and proton density) when a tendon is at a 55° angle to the main magnetic field [12]. This is related to dipolar interactions between water protons in tendon tissue, resulting in T2 relaxation time lengthening [13].

Rotator Cuff Tendon Tears

Rotator cuff tears (Fig. 2) may occur as a result of factors including chronic degeneration and microtrauma and extrinsic compression or impingement of the subacromial space [17]. Rotator cuff tendon tears may be full thickness, extending through the entire short axis of the rotator cuff tendon from the articular to the bursal surface, or partial thickness, involving the bursal or articular side of the tendon only. The diagnosis of rotator cuff tear on MRI is primarily made based on abnormal increased signal on fluid-sensitive images, generally close to fluid signal [16, 18, 19]. Detection of tendon tears on fluid-sensitive imaging is aided by using fat suppression, which increases soft-tissue contrast [20]. In the case of full-thickness tears, the increased signal can bridge between the glenohumeral articular space and the subacromial-subdeltoid bursa. The diagnosis can be more challenging when granulation tissue is associated with the tear, potentially obscuring small full-thickness and partial tears. In this setting, assessing morphology of the rotator cuff tendons is important; signs can include surface contour deformity, myotendinous retraction, and associated subacromial-subdeltoid bursitis [16]. In difficult cases, MR arthrography can confirm small full-thickness tears otherwise obscured by fibrotic tissue [21]. Bony changes of cortical irregularity at the greater tuberosity can provide additional suspicion for an underlying rotator cuff tear, with a 75% positive predictive value for the presence of an associated full- or partial-thickness rotator cuff tear [22].

Rotator cuff full-thickness tears may occur in various patterns [23, 24]. Tears can occur at the insertion or footprint of the rotator cuff or more proximally, frequently about 1 cm proximal to the bony insertion, an area sometimes referred to as the critical zone. Evaluation of rotator cuff tendon tear location, pattern, and extent is important in determining surgical or conservative management. Most commonly, the tear occurs in the short axis of the tendon, in a transverse tear pattern. An L-shaped tear can occur when a transverse tear is combined with a longitudinal-oriented tear component. With retraction of fibers from the insertion of the rotator cuff tendons, a U-shaped pattern can occur, which is relatively difficult to surgically repair.

Massive rotator cuff tears can be defined as those that measure greater than 5 cm or represent a complete tear of two or more tendons [25]. When chronic, these tears are associated with marked rotator cuff muscle atrophy and have poor surgical outcomes. In some cases of massive rotator cuff tear, a bridging appearance can be seen where the retracted tendon ends of two adjacent torn tendons adhere to each other, forming a bridge between the two tendons, for example in the setting of combined subscapularis and supraspinatus tendon tears [26].

Partial-thickness tears involve just one surface of the tendon, either bursal (superficial), or articular (deep), without extending through the entire tendon substance. The depth of a partial-thickness tear should be quantified. This can be graded according to the Ellman classification whereby tears are

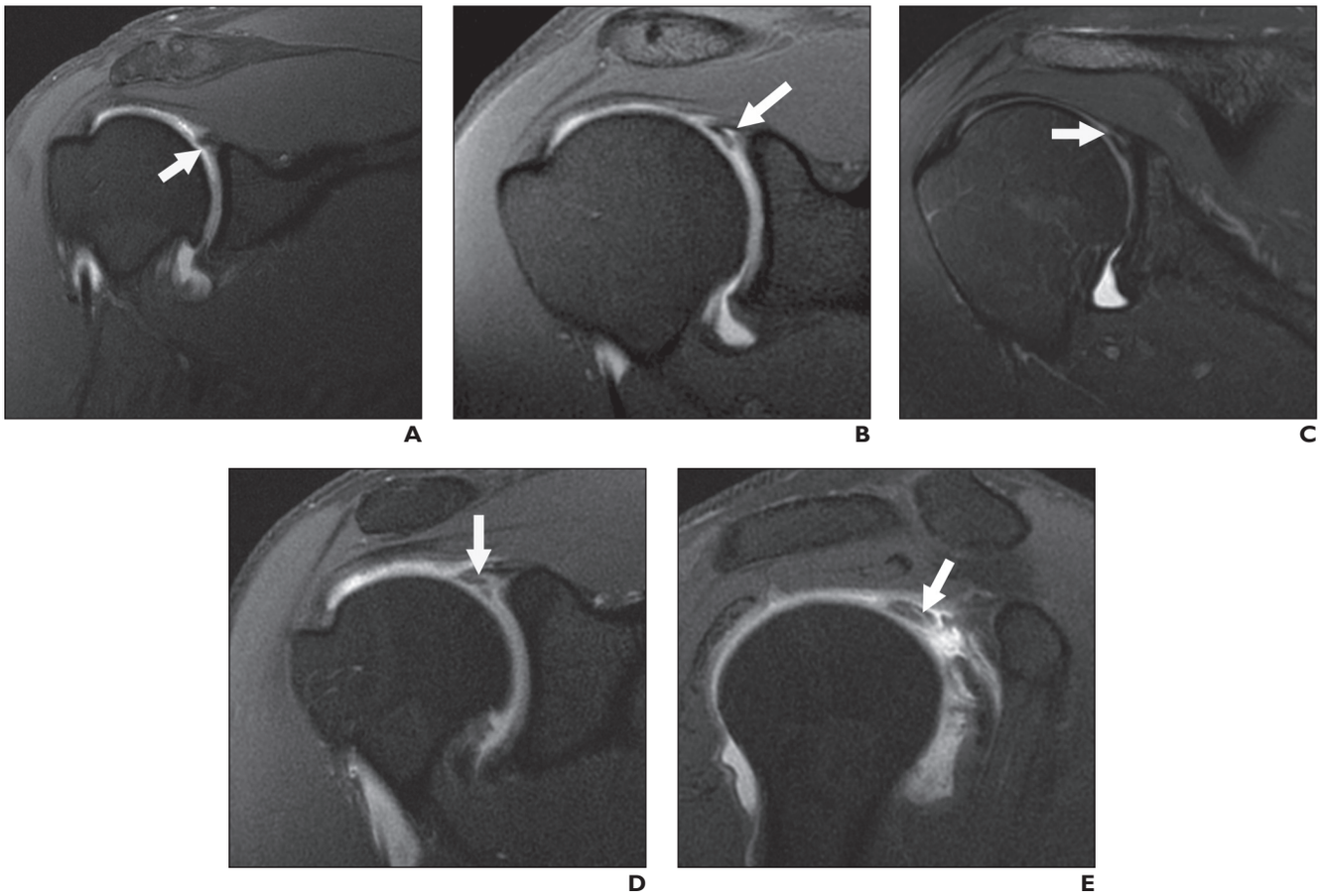

Fig. 6—Superior labral anterior-to-posterior (SLAP) tears.
A, Type I SLAP tear. Coronal fat-suppressed T1-weighted MR arthrogram image shows irregularity and fraying of surface of superior glenoid labrum (*arrow*).
B, Type II SLAP tear. Coronal fat-suppressed T1-weighted MR arthrogram image shows linear high signal undermining superior labrum (*arrow*). Note superolateral orientation of signal away from glenoid.
C, Type III SLAP tear. Coronal T2-weighted image shows high signal transversely oriented within superior labrum (*arrow*), separating labrum into superior and inferior components.
D, Type IV SLAP tear. Coronal fat-suppressed T1-weighted MR arthrogram image shows contrast extending laterally in superior labrum (*arrow*) toward long head of biceps tendon.
E, Type IV SLAP tear. Sagittal fat-suppressed T1-weighted MR arthrogram shows contrast representing extension of superior labral tear into long head of biceps tendon (*arrow*).

classed as grade 1 if less than 3 mm, grade 2 if 3–6 mm, grade 3 if greater than 6 mm [27, 28]. Grade 3 tears typically involve more than half of the tendon. In general, tears of 50% or more are considered for surgical repair, although in some cases, more shallow tears may be helped by arthroscopic debridement [29, 30]. A subtype of articular-sided partial-thickness tears is the rim-rent tear, which refers to a tear at the articular side of the supraspinatus tendon, located at the tendon footprint on the greater tuberosity [31, 32]. This type of tear is most commonly seen in athletes who engage in overhead throwing activities. It is essential to review each rotator cuff tendon on short-axis imaging in addition to its long axis to maximize detection and localization of small tears; for example, assessment of the supraspinatus on oblique sagittal images [33]. The accuracy of MRI for diagnosing partial tendon tears is less than that for full-thickness tears [34, 35]. Small but symptomatic partial articular-sided rotator cuff tears can be better depicted by MRI arthrography, with direct delineation of the tear defect by intraarticular contrast [28, 36, 37].

A discrete subtype of a partial tear is an interstitial or otherwise termed intrasubstance tear. In this case, the tear is confined to within the substance of the tendon, without necessarily surfacing at the bursal or articular side of the tendon. This tear may be occult on arthroscopy and also on MR arthrography unless fluid-sensitive images are acquired in addition to T1-weighted images and thus has also been referred to as a concealed interstitial delamination tear [32]. This tear generally extends along the long axis of the involved tendon and often extends to the tendon footprint. Intrasubstance tears can be isolated or may communicate with partial-thickness bursal, articular, or full-thickness tears [38].

Rotator Cuff Muscles

Muscle Atrophy

Atrophy can be the end result of a variety of processes, but it most commonly occurs as a result of rotator cuff tears. The mechanism of muscle atrophy in this setting is likely a

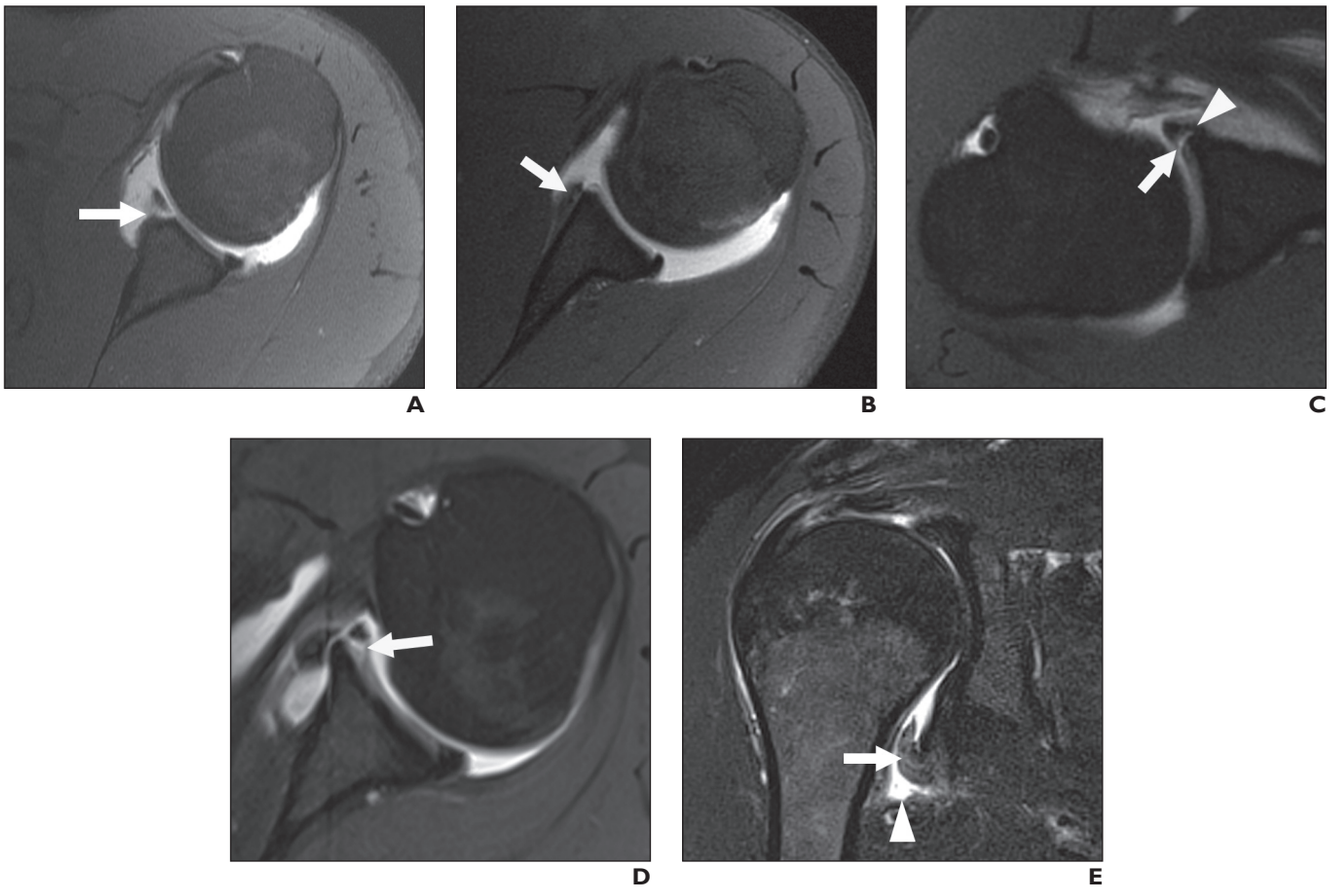

Fig. 7—Labroligamentous injuries.
A, Bankart tear. Axial fat-suppressed MR arthrogram image shows contrast undercutting anterior inferior glenoid labrum (*arrow*), with detachment of periosteum.
B, Anterior labroligamentous periosteal sleeve avulsion. Axial fat-suppressed MR arthrogram image shows medial displacement of anterior inferior labrum (*arrow*) remaining attached to periosteum.
C, Perthes lesion. Axial fat-suppressed MR arthrogram image shows contrast undercutting anterior inferior labrum (*arrow*) but labrum remains attached to glenoid by intact periosteum (*arrowhead*).
D, Glenoid labral articular disruption. Axial fat-suppressed MR arthrogram image shows contrast undercutting glenoid cartilage (*arrow*) in association with adjacent anterior–inferior glenoid labral tear.
E, Humeral avulsion of inferior glenohumeral ligament (IGHL). Coronal fat-suppressed T2-weighted image shows torn IGHL (*arrow*) from its humeral attachment leading to abnormal J-shaped configuration. Note fluid extending though inferior joint capsule (*arrowhead*).

complex effect at a molecular level due to the loss of the normal stimulus of mechanical loading as well as secondary effects on the suprascapular nerve [39]. In general, atrophic muscle undergoes a decrease in volume and replacement of muscle signal with fatty tissue to a varying extent, depending on the severity of atrophy (Fig. 3). Muscle atrophy can be graded in a semiquantitative manner in accordance with the Goutallier grading system [40], originally described for assessment of rotator cuff muscle on CT but widely adopted to MR evaluation. The grading is as follows: grade 0, no fatty deposits; grade 1, some fatty streaks; grade 2, more muscle than fat; grade 3, as much muscle as fat; and grade 4, less muscle than fat.

Detection of muscle atrophy is essential when assessing rotator cuff tears, since presurgical fatty degeneration of rotator cuff muscles is associated with poor surgical outcomes and higher retear rates. Recent work has also explored the use of chemical-shift imaging to provide quantitative assessment of fatty muscle atrophy, permitting calculation of fat fraction and providing potentially more precise and reproducible measurement [41].

Muscle Denervation

Signal changes early in the clinical course of denervation are dominated by increased signal intensity of the denervated muscle (Fig. 4), which is related to altered muscle cell membrane permeability, and enlargement of the intramuscular capillary bed [42]. Denervation also causes proteolysis in skeletal muscle, leading to reduced bulk and replacement of muscle tissue with fat. Denervation of shoulder muscles is not infrequently encountered and follows distinct patterns depending on the nerve involved and the location [43]. The suprascapular nerve passes though fibroosseous tunnels in the suprascapular notch and spinoglenoid notch. Entrapment can occur because of masses, trauma, or ligament hypertrophy. Large paralabral cysts related to an underlying glenoid labral tear may result in compression of the suprascapular nerve, most commonly at the

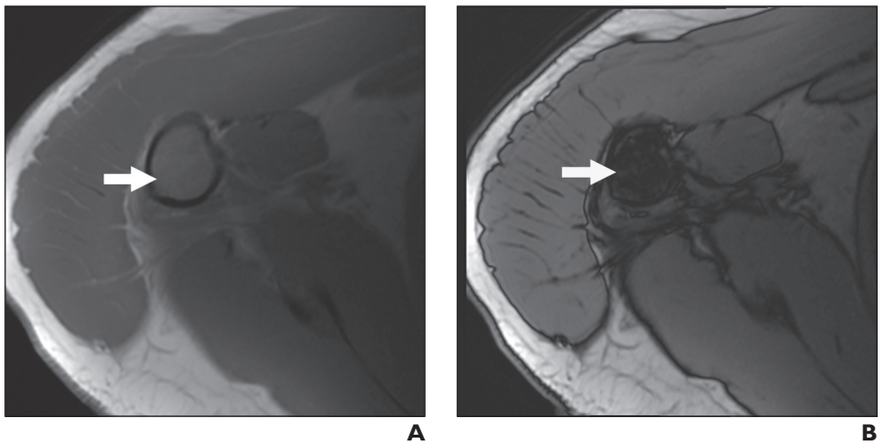

Fig. 8—Bone lesions.
A, Axial in-phase T1-weighted MR image shows bone marrow (*arrow*) relatively low in signal but higher in signal than surrounding muscle.
B, Axial out-of-phase T1-weighted MR image shows marked signal loss compared with in-phase image (**A**), compatible with mixture of fat and water within bone marrow voxels *(arrow)*, typical for hematopoietic red marrow.

spinoglenoid notch. With more proximal compression of the suprascapular nerve there is secondary denervation of both the supraspinatus and infraspinatus muscles, with signal and morphologic changes occurring solely in those muscles. More distal nerve compression on the other hand, at the level of the spinoglenoid notch, leads to isolated denervation of the infraspinatus. Another pattern of denervation around the shoulder is axillary nerve compression in the quadrilateral space. The quadrilateral space is bound laterally by the humerus, medially by the triceps, superiorly by the teres minor, and inferiorly by the teres major. Quadrilateral space syndrome represents compression of the axial nerve in this space, resulting in denervation of the deltoid and teres minor muscles. Finally, Parsonage Turner syndrome is an idiopathic condition that can present with shoulder pain and weakness and results in denervation changes in muscles supplied by the brachial plexus, including the rotator cuff and shoulder girdle [44].

Calcific Tendinitis

Calcific tendinitis of the rotator cuff is an acute painful condition resulting from idiopathic deposition of hydroxyapatite crystals in the rotator cuff tendons or the adjacent subacromial-subdeltoid bursa. Symptoms may resolve spontaneously but in some cases become chronic. Calcific deposits can usually be readily identified on plain radiographs, unless obscured by overlapping structures, as may be the case with deposits anteriorly in the subscapularis tendon (unless an axial view is obtained). In many cases, the diagnosis is not suspected clinically and the patient may present for MRI without a radiograph for correlation, so familiarity with the appearance of this entity on MRI is important. On MR images, calcific deposits can be seen as hypointense foci, usually well-circumscribed, oblong, and varying in size (Fig. 5). They are often associated with swelling of the tendon and subacromial-subdeltoid bursitis, with wall thickening and increased fluid within the subacromial-subdeltoid bursa [45]. In some cases, there can be involvement of the adjacent bone with cortical erosion and extension into the underlying marrow with associated bone marrow edema [46]. In this scenario, the process can be mistaken for malignancy, but the signal pattern and correlation with radiographs can assist in reaching the correct diagnosis.

Labral Disorders

The diagnosis of labral disorders is improved by using MR arthrography over unenhanced MRI [47]. Based on the low incidence of isolated rotator cuff disorders without additional labral injury in younger patients and the high incidence of incidental degenerative tearing in older patients, some advocate the use of MR arthrography routinely in younger patients [48].

Superior Labral Anterior-to-Posterior Tears

Superior labral anterior-to-posterior (SLAP) tears (Fig. 6) can have variable morphology and extent and were initially classified into four subgroups [49, 50]. Type I is fraying of the articular surface of the glenoid labrum. This is visualized on MR arthrogram as irregularity of the superior labral articular surface. Type II is stripping of the superior labrum and attached biceps from the glenoid. In this subtype, contrast undercuts the superior labrum at the glenoid-labral junction and is frequently seen as a laterally oriented abnormal signal on coronal oblique images. Type III is a bucket-handle tear of the superior labrum. This type of tear is characterized by signal on coronal images extending laterally through the superior labrum. A labral fragment may displace inferiorly into the joint (a bucket-handle fragment). This tear, however, spares the long head of biceps tendon. Type IV is a bucket-handle tear involving the long head biceps tendon. This tear is similar to type III with lateral tear extension, but in this case the tear propagates into the long head of biceps tendon origin.

Many other subtypes have been subsequently described [51], but accurate description of morphology and extent of superior labral tears is generally considered more important than the application of more extensive classifications in clinical practice.

It is important to recognize the common normal variation of a sublabral recess at the superior labrum [52]. This recess consists of a potential space undermining the superior labrum located at the anterior half of the superior labrum. It is not seen posterior to the long head of biceps origin. The recess is smooth in contour and extends superomedially for a depth of up to about 14 mm. Recognition of the morphology and orientation of this variant is key to avoid misdiagnosis as SLAP tear [53]. Differentiation is most challenging for type II SLAP tears. Lateral orientation of high signal on oblique coronal images on

MR arthrography in addition to anterior-to-posterior orientation on axial images are helpful features in the diagnosis of a tear rather than a normal recess [54].

Bankart Injuries

Almost 100 years ago, Bankart described an injury of the anterior glenoid labroligamentous complex with variable glenoid bony involvement occurring as a result of traumatic anterior glenohumeral dislocation and resulting in chronic instability [55]. In the classic Bankart injury, the labrum is torn from its glenoid attachment, including avulsion of the periosteum. This can be well depicted on CT or MRI arthrogram with contrast undercutting the torn labrum. A variant of this injury is the anterior labral periosteal sleeve avulsion lesion, where the anterior inferior labrum is torn and displaced medially along the glenoid rim with inferior rotation [56]. In this case, the periosteum remains attached to labrum and bone but is stripped and displaced medially in a sleevelike fashion. Finally, a Perthes lesion consists of an anterior-inferior labral tear with intact but stripped periosteum; correct diagnosis of this tear subtype can be challenging because it may be inconspicuous if nondisplaced or may be mischaracterized as a classic Bankart lesion [57]. Imaging with the patient in abduction and external rotation of the shoulder may improve diagnostic accuracy for Perthes lesions [58].

In patients with Bankart injuries (Fig. 7), CT can provide a useful adjunct to evaluate the extent of bony glenoid injury, and when performed with intraarticular contrast (CT arthrography) can provide accurate assessment of labral, ligamentous, and cartilaginous injury in addition to bony injury characterization [59]. On both CT and MRI, bony injury to the posterior-superior humeral head may be observed (Hill-Sachs injury) in patients who have undergone anterior dislocation of the shoulder. In addition to bony glenoid injuries, there may be combined labral and cartilage injuries, this combination is termed glenolabral articular disruption [60].

The glenohumeral ligaments provide additional important stabilization of the shoulder, and injury due to anterior dislocation may contribute to recurrent shoulder instability. In particular, the inferior glenohumeral ligament (IGHL) is a primary stabilizer in the abducted, externally rotated shoulder. The IGHL is composed of anterior and posterior bands with an axillary pouch between these bands. The normal appearance of the IGHL on coronal MR images is a low-signal, U-shaped structure. In the setting of humeral avulsion of the IGHL, high signal interrupts the humeral attachment (Fig. 7e) and the ligament takes on a J-shaped configuration [61]. On arthrography, intraarticular contrast may extend through this defect in the joint capsule. There may be an associated bony avulsion from the humerus. In some cases, a Bankart-type labral tear may be associated, leading to detachment of the IGHL both medially and laterally, termed a floating anterior IGHL [62]. Alternatively, the IGHL may fail at its glenoid attachment or within its substance [48]. Injury of the IGHL is important to recognize, as failure to include this in surgical management can result in incomplete surgical repair and symptom recurrence after surgery. Associated injuries are common; in particular, subscapularis tears are commonly associated.

Long Head of Biceps Disorders

Similar to other tendons, the long head of the biceps tendon is prone to degeneration (tendinosis) and tearing. Tendinosis is identified by the detection of increased signal intensity within the tendon, often associated with thickening of the tendon. Tearing may be partial, or may be complete, in which case distal retraction is frequently observed, leading to an empty bicipital groove on axial images. It should be noted that long-head biceps tendon disorders have an association with rotator cuff injury, particularly of the subscapularis and supraspinatus tendons [63]. Inflammation of the biceps tendon sheath may also produce anterior shoulder pain and is evidenced on imaging as increased fluid within the tendon sheath. In addition to tears, the long head of the biceps tendon may undergo medial dislocation. This is typically in association with subscapularis tendon injury [64]. The resultant malposition of the tendon with respect to the subscapularis depends on the pattern of associated subscapularis injury. When the subscapularis tendon is completely torn, the long head of the biceps tendon is usually displaced deep to the subscapularis. With oblique full-thickness tears of the subscapularis, the tendon may be deep to the subscapularis superiorly, interdigitate with the subscapularis midfibers, and superficial to the inferior subscapularis fibers.

Bone Lesions

Many bone lesions can potentially occur about the shoulder. A description of the myriad of potential lesions is beyond the scope of this review, but it is important to be vigilant in reviewing the bony structures of the shoulder in every case, as shoulder pain can be a presenting complaint for lesions ranging from primary to secondary neoplasm and clinically may be mistaken for a soft tissue injury. A common conundrum encountered on MRI of the shoulder is areas of heterogeneous marrow noted incidentally, raising concern for an underlying bone lesion. In many cases, areas of relatively low signal can be attributed to hematopoietic red marrow. To make this diagnosis, it is essential to review T1-weighted images without fat suppression (which should be included in the imaging protocol). On routine T1-weighted images, hematopoietic marrow is usually hyperintense to skeletal muscle [65]. Chemical-shift imaging can be used in problematic cases to confirm the diagnosis of hematopoietic marrow. Typically, hematopoietic bone marrow signal is lower on opposed-phase T1-weighted images when compared with in-phase images (Fig. 8). This can be assessed quantitatively as a relative signal ratio, defined as the lesion to muscle ratio on opposed-phase divided by lesion to muscle ratio on in-phase images, respectively. Red marrow will usually have a relative signal intensity ratio of less than 0.8 [66].

Conclusion

MRI shows high accuracy in diagnosing causes of shoulder pain, including rotator cuff injuries, glenohumeral or acromioclavicular arthropathy, and labral tears. Pretest evaluation to establish the clinical differential diagnosis permits appropriate imaging technique planning. In view of the high sensitivity of MRI and high prevalence of shoulder disorders in adult populations, clinical evaluation remains central

to determining patient management and integrating the clinical relevance of findings on shoulder MRI [67]. The decision regarding the need for surgical intervention is personalized to individual patients, with specific regard to patient activity level and demographics in addition to consideration of imaging patterns of injury [68].

REFRENCES

1. Boström M, Dellve L, Thomée S, Hagberg M. Risk factors for generally reduced productivity–a prospective cohort study of young adults with neck or upper-extremity musculoskeletal symptoms. *Scand J Work Environ Health* 2008; 34:120–132
2. Virta L, Joranger P, Brox JI, Eriksson R. Costs of shoulder pain and resource use in primary health care: a cost-of-illness study in Sweden. *BMC Musculoskelet Disord* 2012; 13:17
3. Brox JI. Shoulder pain. *Best Pract Res Clin Rheumatol* 2003; 17:33–56
4. Shanahan EM, Sladek R. Shoulder pain at the workplace. *Best Pract Res Clin Rheumatol* 2011; 25:59–68
5. Silverstein BA, Bao SS, Fan ZJ, et al. Rotator cuff syndrome: personal, work-related psychosocial and physical load factors. *J Occup Environ Med* 2008; 50:1062–1076
6. Valkering KP, Stokman RD, Bijlsma TS, Brohet RM, van Noort A. Prevalence of symptomatic rotator cuff ruptures after shoulder trauma: a prospective cohort study. *Eur J Emerg Med* 2014; 21:349–353
7. Teunis T, Lubberts B, Reilly BT, Ring D. A systematic review and pooled analysis of the prevalence of rotator cuff disease with increasing age. *J Shoulder Elbow Surg* 2014; 23:1913–1921
8. Ensor KL, Kwon YW, Dibeneditto MR, Zuckerman JD, Rokito AS. The rising incidence of rotator cuff repairs. *J Shoulder Elbow Surg* 2013; 22:1628–1632
9. White JJ, Titchener AG, Fakis A, Tambe AA, Hubbard RB, Clark DI. An epidemiological study of rotator cuff pathology using The Health Improvement Network database. *Bone Joint J* 2014; 96-B:350–353
10. Mather RC 3rd, Koenig L, Acevedo D, et al. The societal and economic value of rotator cuff repair. *J Bone Joint Surg Am* 2013; 95:1993–2000
11. Moosmayer S, Lund G, Seljom US, et al. Tendon repair compared with physiotherapy in the treatment of rotator cuff tears: a randomized controlled study in 103 cases with a five-year follow-up. *J Bone Joint Surg Am* 2014; 96:1504–1514
12. Timins ME, Erickson SJ, Estkowski LD, Carrera GF, Komorowski RA. Increased signal in the normal supraspinatus tendon on MR imaging: diagnostic pitfall caused by the magic-angle effect. *AJR* 1995; 165:109–114
13. Hayes CW, Parellada JA. The magic angle effect in musculoskeletal MR imaging. *Top Magn Reson Imaging* 1996; 8:51–56
14. Khan KM, Cook JL, Bonar F, Harcourt P, Astrom M. Histopathology of common tendinopathies. Update and implications for clinical management. *Sports Med* 1999; 27:393–408
15. Zlatkin MB, Reicher MA, Kellerhouse LE, McDade W, Vetter L, Resnick D. The painful shoulder: MR imaging of the glenohumeral joint. *J Comput Assist Tomogr* 1988; 12:995–1001
16. Rafii M, Firooznia H, Sherman O, et al. Rotator cuff lesions: signal patterns at MR imaging. *Radiology* 1990; 177:817–823
17. Yadav H, Nho S, Romeo A, MacGillivray JD. Rotator cuff tears: pathology and repair. *Knee Surg Sports Traumatol Arthrosc* 2009; 17:409–421
18. Evancho AM, Stiles RG, Fajman WA, et al. MR imaging diagnosis of rotator cuff tears. *AJR* 1988; 151:751–754
19. Kneeland JB, Middleton WD, Carrera GF, et al. MR imaging of the shoulder: diagnosis of rotator cuff tears. *AJR* 1987; 149:333–337
20. Quinn SF, Sheley RC, Demlow TA, Szumowski J. Rotator cuff tendon tears: evaluation with fat-suppressed MR imaging with arthroscopic correlation in 100 patients. *Radiology* 1995; 195:497–500
21. Magee T. MR versus MR arthrography in detection of supraspinatus tendon tears in patients without previous shoulder surgery. *Skeletal Radiol* 2014; 43:43–48
22. Wohlwend JR, van Holsbeeck M, Craig J, et al. The association between irregular greater tuberosities and rotator cuff tears: a sonographic study. *AJR* 1998; 171:229–233
23. Sallay PI, Hunker PJ, Lim JK. Frequency of various tear patterns in full-thickness tears of the rotator cuff. *Arthroscopy* 2007; 23:1052–1059
24. Gyftopoulos S, Beltran LS, Gibbs K, et al. Rotator cuff tear shape characterization: a comparison of two-dimensional imaging and three-dimensional magnetic resonance reconstructions. *J Shoulder Elbow Surg* 2016; 25:22–30
25. Thes A, Hardy P, Bak K. Decision-making in massive rotator cuff tear. *Knee Surg Sports Traumatol Arthrosc* 2015; 23:449–459
26. Jung JY, Yoon YC, Cha DI, Yoo JC, Jung JY. The "bridging sign": a MR finding for combined full-thickness tears of the subscapularis tendon and the supraspinatus tendon. *Acta Radiol* 2013; 54:83–88
27. Ellman H. Diagnosis and treatment of incomplete rotator cuff tears. *Clin Orthop Relat Res* 1990; 64–74
28. Waldt S, Bruegel M, Mueller D, et al. Rotator cuff tears: assessment with MR arthrography in 275 patients with arthroscopic correlation. *Eur Radiol* 2007; 17:491–498
29. Franceschi F, Papalia R, Del Buono A, Maffulli N, Denaro V. Repair of partial tears of the rotator cuff. *Sports Med Arthrosc Rev* 2011; 19:401–408
30. Payne LZ, Altchek DW, Craig EV, Warren RF. Arthroscopic treatment of partial rotator cuff tears in young athletes. A preliminary report. *Am J Sports Med* 1997; 25:299–305
31. Tuite MJ, Turnbull JR, Orwin JF. Anterior versus posterior, and rim-rent rotator cuff tears: prevalence and MR sensitivity. *Skeletal Radiol* 1998; 27:237–243
32. Schaeffeler C, Mueller D, Kirchhoff C, Wolf P, Rummeny EJ, Woertler K. Tears at the rotator cuff footprint: prevalence and imaging characteristics in 305 MR arthrograms of the shoulder. *Eur Radiol* 2011; 21:1477–1484
33. Tuite MJ, Asinger D, Orwin JF. Angled oblique sagittal MR imaging of rotator cuff tears: comparison with standard oblique sagittal images. *Skeletal Radiol* 2001; 30:262–269
34. Balich SM, Sheley RC, Brown TR, Sauser DD, Quinn SF. MR imaging of the rotator cuff tendon: interobserver agreement and analysis of interpretive errors. *Radiology* 1997; 204:191–194
35. Lenza M, Buchbinder R, Takwoingi Y, Johnston RV, Hanchard NC, Faloppa F. Magnetic resonance imaging, magnetic resonance arthrography and ultrasonography for assessing rotator cuff tears in people with shoulder pain for whom surgery is being considered. *Cochrane Database Syst Rev* 2013; CD009020
36. Meister K, Thesing J, Montgomery WJ, Indelicato PA, Walczak S, Fontenot W. MR arthrography of partial thickness tears of the undersurface of the rotator cuff: an arthroscopic correlation. *Skeletal Radiol* 2004; 33:136–141
37. de Jesus JO, Parker L, Frangos AJ, Nazarian LN. Accuracy of MRI, MR arthrography, and ultrasound in the diagnosis of rotator cuff tears: a meta-analysis. *AJR* 2009; 192:1701–1707
38. Choo HJ, Lee SJ, Kim JH, et al. Delaminated tears of the rotator cuff: prevalence, characteristics, and diagnostic accuracy using indirect MR arthrography. *AJR* 2015; 204:360–366
39. Laron D, Samagh SP, Liu X, Kim HT, Feeley BT. Muscle degeneration in rotator cuff tears. *J Shoulder Elbow Surg* 2012; 21:164–174
40. Goutallier D, Postel JM, Gleyze P, Leguilloux P, Van Driessche S. Influence of cuff muscle fatty degeneration on anatomic and functional outcomes after simple suture of full-thickness tears. *J Shoulder Elbow Surg* 2003; 12:550–554
41. Lee S, Lucas RM, Lansdown DA, et al. Magnetic resonance rotator cuff fat fraction and its relationship with tendon tear severity and subject characteristics. *J Shoulder Elbow Surg* 2015; 24:1442–1451
42. Kamath S, Venkatanarasimha N, Walsh MA, Hughes PM. MRI appearance of muscle denervation. *Skeletal Radiol* 2008; 37:397–404
43. Yanny S, Toms AP. MR patterns of denervation around the shoulder. *AJR* 2010; 195:[web]W157-W163
44. Scalf RE, Wenger DE, Frick MA, Mandrekar JN, Adkins MC. MRI findings of 26 patients with Parsonage-Turner syndrome. *AJR* 2007; 189:[web]W39-W44
45. Zubler C, Mengiardi B, Schmid MR, Hodler J, Jost B, Pfirrmann CW. MR arthrography in calcific tendinitis of the shoulder: diagnostic performance and pitfalls. *Eur Radiol* 2007; 17:1603–1610
46. Flemming DJ, Murphey MD, Shekitka KM, Temple HT, Jelinek JJ, Kransdorf MJ. Osseous involvement in calcific tendinitis: a retrospective review of 50 cases. *AJR* 2003; 181:965–972
47. Flannigan B, Kursunoglu-Brahme S, Snyder S, Karzel R, Del Pizzo W, Resnick D. MR arthrography of the shoulder: comparison with conventional MR imaging. *AJR* 1990; 155:829–832
48. Roy EA, Cheyne I, Andrews GT, Forster BB. Beyond the Cuff: MR Imaging of Labroligamentous Injuries in the Athletic Shoulder. *Radiology* 2016; 278:316–332 [Erratum in *Radiology* 2016; 279:328]
49. Cartland JP, Crues JV 3rd, Stauffer A, Nottage W, Ryu RK. MR imaging in the evaluation of SLAP injuries of the shoulder: findings in 10 patients. *AJR* 1992; 159:787–792
50. Snyder SJ, Karzel RP, Del Pizzo W, Ferkel RD, Friedman MJ. SLAP lesions of the shoulder. *Arthroscopy* 1990; 6:274–279
51. Modarresi S, Motamedi D, Jude CM. Superior labral anteroposterior lesions of the shoulder: part 2, mechanisms and classification. *AJR* 2011; 197:604–611
52. Smith DK, Chopp TM, Aufdemorte TB, Witkowski EG, Jones RC. Sublabral recess of the superior glenoid labrum: study of cadavers with conventional nonenhanced MR imaging, MR arthrography, anatomic dissection, and limited histologic examination. *Radiology* 1996; 201:251–256
53. Bencardino JT, Beltran J, Rosenberg ZS, et al. Superior labrum anterior-posterior lesions: diagnosis with MR arthrography of the shoulder. *Radiology* 2000; 214:267–271
54. Jin W, Ryu KN, Kwon SH, Rhee YG, Yang DM. MR arthrography in the differential diagnosis of type II superior labral anteroposterior lesion and sublabral recess. *AJR* 2006; 187:887–893

55. Bankart AS. Recurrent or habitual dislocation of the shoulder-joint. *BMJ* 1923; 2:1132–1133
56. Neviaser TJ. The anterior labroligamentous periosteal sleeve avulsion lesion: a cause of anterior instability of the shoulder. *Arthroscopy* 1993; 9:17–21
57. Waldt S, Burkart A, Imhoff AB, Bruegel M, Rummeny EJ, Woertler K. Anterior shoulder instability: accuracy of MR arthrography in the classification of anteroinferior labroligamentous injuries. *Radiology* 2005; 237:578–583
58. Tian CY, Cui GQ, Zheng ZZ, Ren AH. The added value of ABER position for the detection and classification of anteroinferior labroligamentous lesions in MR arthrography of the shoulder. *Eur J Radiol* 2013; 82:651–657
59. Acid S, Le Corroller T, Aswad R, Pauly V, Champsaur P. Preoperative imaging of anterior shoulder instability: diagnostic effectiveness of MDCT arthrography and comparison with MR arthrography and arthroscopy. *AJR* 2012; 198:661–667
60. Neviaser TJ. The GLAD lesion: another cause of anterior shoulder pain. *Arthroscopy* 1993; 9:22–23
61. Bui-Mansfield LT, Taylor DC, Uhorchak JM, Tenuta JJ. Humeral avulsions of the glenohumeral ligament: imaging features and a review of the literature. *AJR* 2002; 179:649–655
62. Bui-Mansfield LT, Banks KP, Taylor DC. Humeral avulsion of the glenohumeral ligaments: the HAGL lesion. *Am J Sports Med* 2007; 35:1960–1966
63. Beall DP, Williamson EE, Ly JQ, et al. Association of biceps tendon tears with rotator cuff abnormalities: degree of correlation with tears of the anterior and superior portions of the rotator cuff. *AJR* 2003; 180:633–639
64. Tuckman GA. Abnormalities of the long head of the biceps tendon of the shoulder: MR imaging findings. *AJR* 1994; 163:1183–1188
65. Carroll KW, Feller JF, Tirman PF. Useful internal standards for distinguishing infiltrative marrow pathology from hematopoietic marrow at MRI. *J Magn Reson Imaging* 1997; 7:394–398
66. Disler DG, McCauley TR, Ratner LM, Kesack CD, Cooper JA. In-phase and out-of-phase MR imaging of bone marrow: prediction of neoplasia based on the detection of coexistent fat and water. *AJR* 1997; 169:1439–1447
67. Magee T. How often do surgeons intervene on shoulder labral lesions detected at MR examination? A retrospective review of MR examinations correlated with arthroscopy. *Br J Radiol* 2014; 87:20130736
68. Kweon C, Gagnier JJ, Robbins CB, Bedi A, Carpenter JE, Miller BS. Surgical versus nonsurgical management of rotator cuff tears: predictors of treatment allocation. *Am J Sports Med* 2015; 43:2368–2372